CHEMISTRY OF MATERIALS

Article

pubs.acs.org/cm

Controlling C_{60} Organization through Dipole-Induced Band Alignment at Self-Assembled Monolayer Interfaces

Mohamed A. Mezour,[†] Oleksandr Voznyy,[‡] Edward H. Sargent,[‡] R. Bruce Lennox,*[,†] and Dmitrii F. Perepichka*[,†]

[†]Department of Chemistry and Centre for Self-Assembled Chemical Structures, McGill University, 801 Sherbrooke Street West, Montreal, Quebec H3A 0B8, Canada

[‡]The Edward S. Rogers Department of Electrical and Computer Engineering, University of Toronto, 10 King's College Road, Toronto, Ontario M5S 3G4, Canada

Supporting Information

ABSTRACT: Understanding the structural organization and growth of organic molecules on self-assembled monolayers (SAMs) is crucial for creating high-performance SAM-based electronic devices. We report herein C_{60} adsorption onto benzenethiol (BT), pentafluorobenzenethiol (PFBT), and octanethiol (C8SH) SAM-modified Au(111) studied using scanning tunneling microscopy at the liquid–solid interface. A continuous film of C_{60} molecules forms at a much faster rate ($k = 3.3 \times 10^{-7}$ s^{-1}) on PFBT compared to that on BT ($k = 7.2 \times 10^{-9}$ s^{-1}) and C8SH SAMs ($k = 9.5 \times 10^{-9}$ s^{-1}). On the basis of density functional theory calculations, we propose that the difference in C_{60} growth behavior originates from the dipole-induced dipole interactions between the SAM and C_{60}. This may be further augmented by an inverse charge transfer from C_{60} to SAM. This work provides new insights into the self-assembly behavior of next-generation electronic materials.

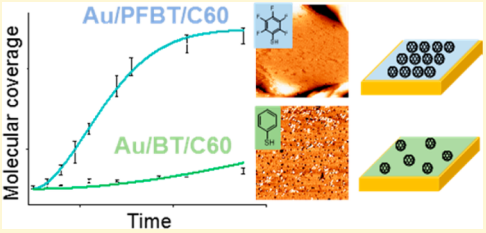

Self-assembled monolayers (SAMs) prepared from thiol-terminated molecules have been successfully used to tailor the physical and chemical properties of metals and semiconductors[1−3] for a range of applications, including electrochemical sensors,[4] surface patterning,[5] friction and lubrication control,[6] and protective coatings.[7] SAMs also offer a ready means for tuning the work function of an electrode, reducing the charge injection barrier between the electrode and the semiconductor, and controlling the morphology of the semiconductor films grown on such functionalized surfaces. For this reason, SAMs have become an integral part of many organic semiconducting devices, including organic light-emitting diodes (OLEDs), field-effect transistors (OFETs), and solar cells.[8−11]

Alkanethiols with different chain lengths[12] and their fluorinated derivatives[13] have been used to modify the surface potential of metal substrates and their interaction with organic semiconductors. However, the large band gap of the aliphatic thiols (>5 eV) limits the charge transport across the resulting SAMs, which may be detrimental to device performance.[14] On the other hand, aromatic thiols[15] can facilitate charge transfer across the SAMs and be highly effective in tuning the energy level alignment/reducing contact resistance at the metal–semiconductor interface. The substituents in the aromatic ring can be used to tune and even invert the surface dipole (μ). The work function of a Au electrode can thus be shifted by approximately −0.3 to −0.6 eV and +0.7 eV using benzenethiol (BT; $\mu = -2.4$ D) and pentafluorobenzenethiol (PFBT; $\mu = +3.5$ D) SAMs, respectively.[16,17] PFBT has been widely used in contact engineering in organic electronics.[11,18−22] Its role in improving charge transport is not yet fully understood and has been attributed to a reduced charge injection barrier,[18,21] surface hydrophobicity (repelling charge trap impurities such as water),[22] a change in the semiconductor film morphology/molecular orientation,[19,20,22] and specific F···F and F···S interactions with semiconducting molecules.[23]

Buckminsterfullerene (C_{60}) is one of the most remarkable n-type organic semiconductors for a number of applications, including single-molecule[24] and thin film organic electronic devices.[25,26] Much effort has been devoted to understanding and controlling the assembly of C_{60} in thin film devices such as solar cells.[27] Consequently, the molecular orientation and supramolecular organization of C_{60} monolayers on metals (Au,[28,29] Ag,[29,30] and Cu[31]), inorganic (ZnO,[32] TiO_2,[33] and Si[34]) and organic (porphyrins,[35] oligothiophenes,[36,37] and pentacene[38]) semiconductors have been studied extensively. In contrast, adsorption of C_{60} onto organothiols has rarely been explored. Vapor deposition of C_{60} on alkanethiol SAMs leads to closely packed islands[39] or one-dimensional chains[40] that were thought to reside on top of the SAM molecules. C_{60} penetration and intermixing with octanethiol[41] and 11-phenoxyundecanethiol SAMs[42] were also suggested.

Here we report the first study of adsorption of fullerene C_{60} onto aromatic SAMs. Using *in situ* scanning tunneling microscopy (STM) at the liquid–solid interface, we compare

Received: August 22, 2016
Revised: October 7, 2016
Published: October 10, 2016

© 2016 American Chemical Society

DOI: 10.1021/acs.chemmater.6b03527
Chem. Mater. 2016, 28, 8322−8329

the structural properties of BT and PFBT on Au(111) and measure the kinetics of the adsorption of C_{60} on BT, PFBT, and octanethiol (C8SH) SAMs, as well as bare Au(111). Through X-ray photoelectron spectroscopy (XPS) measurements, we demonstrate that, in contrast to previous reports,[41,42] the C_{60} does not displace the thiol molecules during adsorption but forms an adlayer on top of the SAM. The significant enhancement of the adsorption of C_{60} on PFBT versus BT or C8SH SAMs is counterintuitive as it suggests a higher lipophilicity of the fluorinated SAM. The observed phenomenon is investigated using density functional theory (DFT) calculations and explained in terms of dipole (PFBT)−induced dipole (C_{60}) interaction.

RESULTS

Self-Assembly of PFBT and BT on Au(111). The electronic properties of BT and PFBT SAMs, especially their surface potential, are related to their structural order and molecular coverage.[43] The study of the structure and molecular orientation of these SAMs thus provides an opportunity to investigate the effect of different dipole moments within SAMs on the morphology of subsequent organic layers.

The self-assembly of BT[44−48] and PFBT[49,50] on Au(111) has been studied using various analytical techniques. For instance, STM characterization of BT adsorption at room temperature reveals either completely disordered SAM[44] or small ordered domains (<15 nm^2).[46] BT and PFBT SAMs with different structural lattices (Table S1) have been observed under specific preparation conditions (e.g., long incubation time of 190 h,[49] elevated temperature of 75 °C,[47,50] and exchange with a preadsorbed cyclohexanethiol SAM[48]). Such a dependence of the SAM structure on the preparation mode, and the variety of contradictory reports, complicate comparisons between BT and PFBT SAMs and prompted us to perform the comparative studies under identical conditions.

Figures 1 and 2 show representative STM images at the air−solid interface of SAMs prepared by immersion of Au(111) in ethanol solutions of BT and PFBT (1 mM) for 18 h at 60 °C. BT and PFBT form structural domains consisting of ordered molecular size features. One can distinguish pits and islands with an apparent STM height of approximately ±2.4 Å that corresponds to the height of a monatomic Au(111) layer (Figure S1). While their occurrence was somewhat dependent on sample preparation, we typically observed pit defects for BT SAMs and island defects for PFBT SAMs. Pits and islands have been previously observed on BT and PFBT SAMs, respectively, and were attributed to the relaxation of the herringbone reconstruction of Au(111) and the release of Au adatoms.[48,49,45] The mobility of these adatoms, controlled by the nature of SAM molecules, determines whether islands or pits are preferentially formed.[45]

The BT and PFBT molecules are resolved as bright spots forming parallel stripes oriented along one of the three preferential $\langle 1\bar{1}0 \rangle$ directions reflecting the 3-fold symmetry of the underlying Au(111) (Figures 1a and 2a). High-resolution STM images of BT SAMs reveal the formation of two different phases, in an ∼1:3 ratio, here termed the α phase and β phase (Figure 1b,c). The α phase is described by an oblique unit cell that contains one molecule and has the following parameters: $a = b = 0.54 \pm 0.1$ nm, and $\gamma = 63 \pm 3°$. A comparison of the dimensions and orientation of the unit cell with the underlying Au(111) lattice suggests an $a_h(\sqrt{3} \times \sqrt{3})R30°$ commensurate structure, where the a_h value of 2.89 Å is the closest neighbor interatomic distance in the Au[111] plane. This unit cell is consistent with a herringbone-like arrangement of BT molecules, a packing mode frequently observed for aromatic thiols.[45]

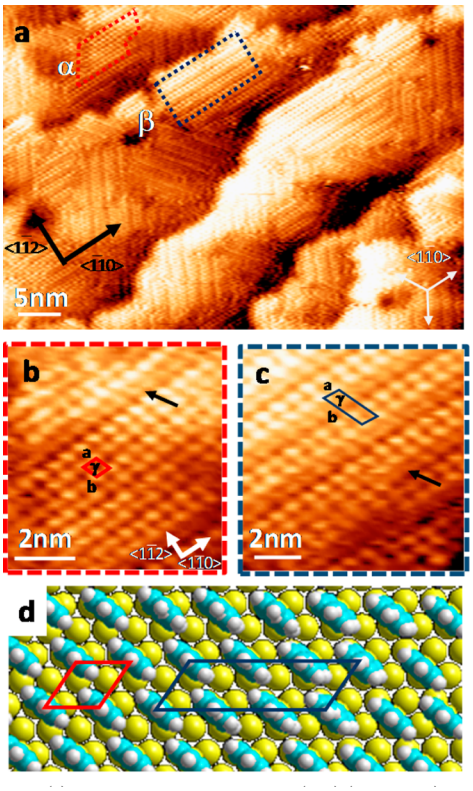

Figure 1. (a) STM image of BT SAMs on Au(111) (54 nm × 40 nm). The red and blue dashed rectangles highlight α and β phases, respectively. (b and c) High-resolution STM images of α and β phases of BT SAM, respectively (7 nm × 7 nm). Unit cell for the α phase is as follows: $a = b = 0.54 \pm 0.1$ nm, and $\gamma = 63 \pm 3°$. Unit cell for the β phase is as follows: $a = 0.52 \pm 0.1$ nm, $b = 1.5 \pm 0.1$ nm, and $\gamma = 63 \pm 3°$. (d) Molecular model of BT SAM. $V_b = 200$ mV, and $I_t = 0.2$ nA.

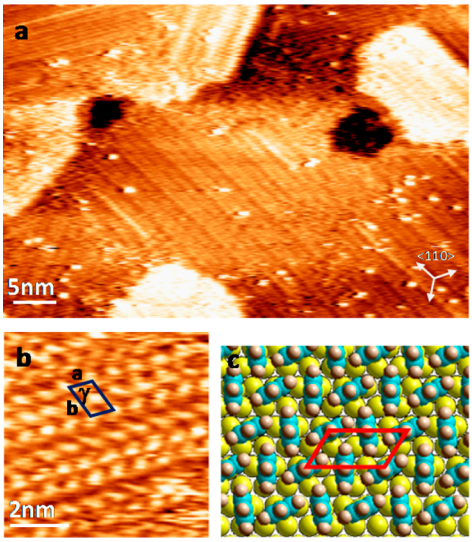

Figure 2. (a) Large scale STM image of PFBT SAMs on Au(111) (54 nm × 40 nm). (b) High-resolution STM image (7 nm × 7 nm) of PFBT SAM, with the following unit cell: $a = 0.58 \pm 0.1$ nm, $b = 0.98 \pm 0.1$ nm, and $\gamma = 64 \pm 4°$. (c) Molecular model of PFBT SAM. $V_b = 200$ mV, and $I_t = 0.2$ nA.

DOI: 10.1021/acs.chemmater.6b03527
Chem. Mater. 2016, 28, 8322−8329

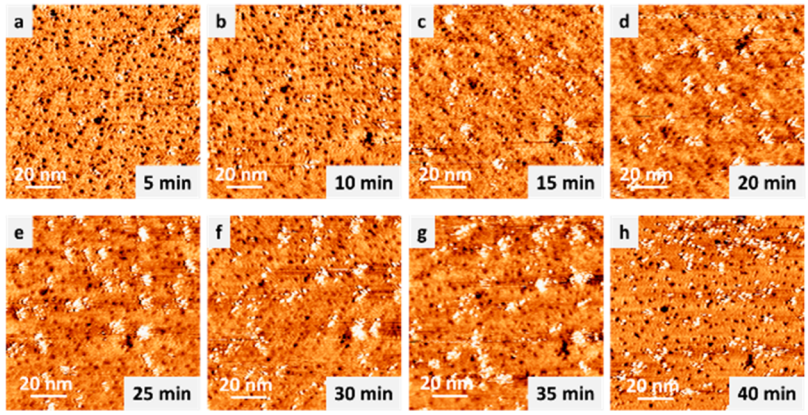

Figure 3. Sequential STM images recorded in 1 mM C_{60}/phenyloctane on BT SAM-modified Au(111). V_b = 400 mV, and I_t = 0.2 nA.

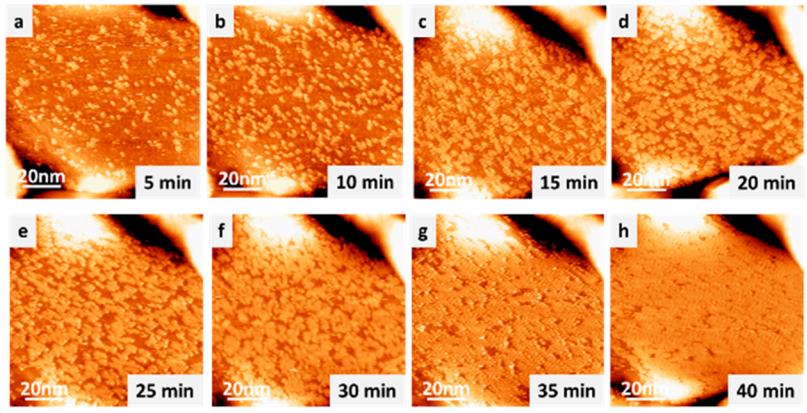

Figure 4. Sequence of STM images recorded in 1 mM C_{60}/phenyloctane on PFBT SAM-modified Au(111). V_b = 400 mV, and I_t = 0.2 nA.

In the β phase, each third stripe appears with a lower brightness (lower STM height), which results in a unit cell that contains three molecules and has the following parameters: a = 0.52 ± 0.1 nm, b = 1.5 ± 0.1 nm, and γ = 63 ± 3°. This suggests an $a_h(\sqrt{3} \times 3\sqrt{3})$R30° structure relative to the Au(111) lattice. The unit cells of the α and β phases are commensurable along both a and b directions and differ only in molecular contrast. A possible origin of this contrast difference could be the presence of Au adatoms[51] or, more likely, different orientations of the molecular plane with respect to the unit cell vectors. Occasionally, contrast switching either within or between the adjacent molecular rows (black arrows in Figure 1b,c) has been observed upon sequential imaging (Figure S2).

A high-resolution STM image of PFBT SAMs shows a long-range ordered structure (a = 0.58 ± 0.1 nm, b = 0.98 ± 0.1 nm, and γ = 62 ± 2°) containing two nonequivalent molecules. This likely corresponds to the commensurate structure $a_h(\sqrt{3} \times 2\sqrt{3})$R30° (Figure 1b). In contrast to that of BT SAM, the herringbone-like arrangement of PFBT molecules is clearly identified from the high-resolution STM image, which might be attributed to the reduced rotational mobility of the larger PFBT molecules.

Overall, BT (α and β phases) and PFBT SAMs show the same (within experimental uncertainty) two-dimensional (2D) lattice that is described by a commensurate $(m\sqrt{3} \times n\sqrt{3})$R30° structure ($m$ and n are integers). Their differences (see below) thus must be ascribed exclusively to electronic effects.

Self-Assembly of C_{60} on SAM-Modified Au(111). Figures 3 and 4 and Figure S3 show sequential constant current STM images following the addition of a C_{60} solution in phenyloctane (~1 mM) on BT and PFBT, respectively (STM movies are available in the Supporting Information). All the following STM measurements were taken at a liquid−solid interface. Adsorption of C_{60} on a BT SAM initially results in isolated bright spots with an apparent height of ~4 Å and a lateral size of ~1 nm, which could be attributed to individual fullerenes (Figure 3).[52] Their population increases with time, and small aggregates of 2−5 nm become visible after ~10 min; however, no continuous monolayer is formed. Similarly, only disordered aggregates of C_{60} have been observed on C8SH-Au (Figure S3).

However, the behavior of C_{60} on the PFBT SAM is very different. Bright islands 2−6 nm in size are formed within 5 min, and their size continues to increase until a full monolayer is formed within ~40 min (Figure 4). The analysis of the height profile of C_{60} on PFBT (Figure 5 and Figure S4a) shows an apparent height of 0.4 ± 0.1 nm, similar to the height measured for C_{60} on BT and C8SH SAMs (Figure S4b). Occasional areas with a double height (0.9 ± 0.1 nm) are attributed to two C_{60} layers.

An inspection of the spatial distribution of C_{60} molecules in the second layer reveals that they are preferentially located at the edges of the underlying C_{60} islands (Figure 5). This suggests a mechanism by which C_{60} monolayer formation is initiated by nucleation and growth of 2D islands in the submonolayer regime, and then the subsequent C_{60} molecules adsorb either on free Au or on top of the C_{60} domains where they diffuse to edges and cross the step-edge (Ehrlich−Schwoebel) barrier[53] contributing to the complete formation of the monolayer.[54,55]

DOI: 10.1021/acs.chemmater.6b03527
Chem. Mater. 2016, 28, 8322−8329

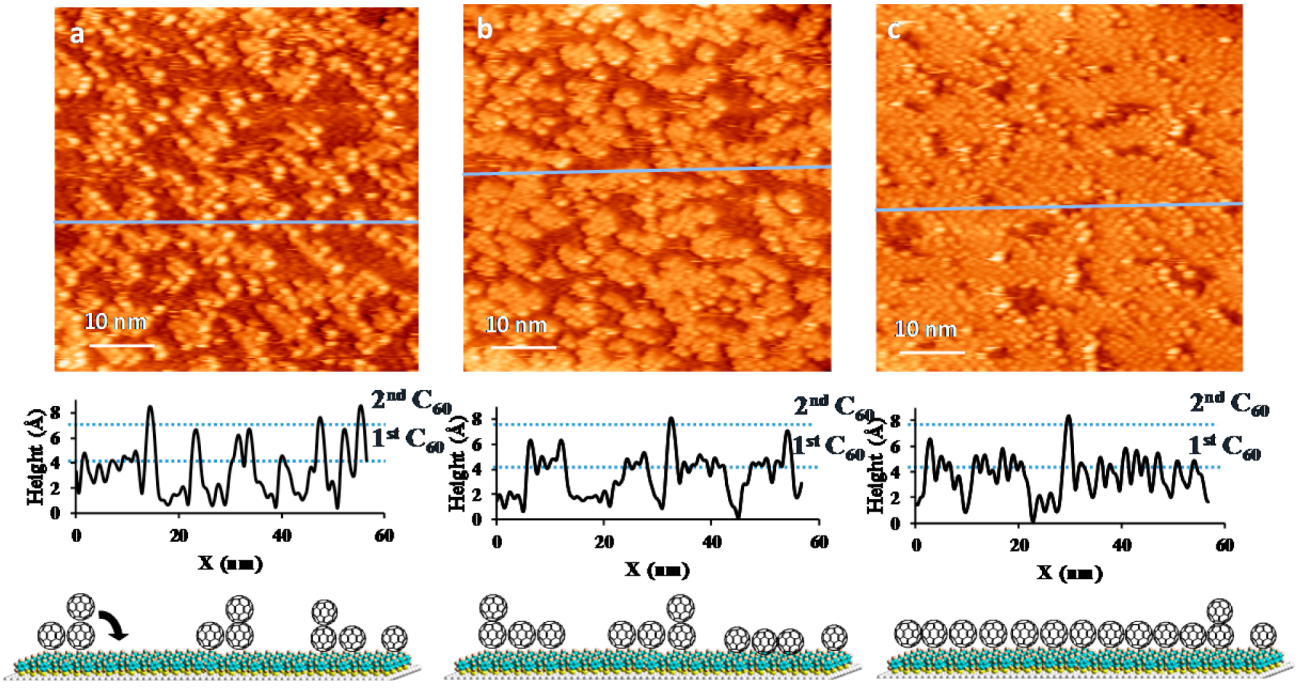

Figure 5. STM images and surface profile of the growing C_{60} film on PFBT-modified Au(111) after (a) 15, (b) 25, and (c) 35 min. Area of 57 nm × 57 nm. V_b = 400 mV, and I_t = 0.2 nA.

Further STM investigation of the assembly of C_{60} on top of PFBT SAM reveals a closely packed hexagonal lattice with the following unit cell dimensions: $a = b = 1.0 \pm 0.2$ nm, and $\alpha = 60 \pm 2°$ [assigned to the $(2\sqrt{3} \times 2\sqrt{3})R30°$ structure (Figure 6)]. Similar packing has also been observed for C_{60} adsorbed on bare gold at the phenyloctane−Au interface ($a = b = 1.07 \pm 0.1$ nm, and $\alpha = 63 \pm 3°$) (Figure S5).

An enhanced adsorption of C_{60} was also observed on 4-chlorobenzenethiol SAM, although the resulting fullerene adlayer appears to be less ordered than that on PFBT (Figure S10).

DISCUSSION

We first ask whether PFBT molecules remain intact upon C_{60} adsorption. Recent literature on C_{60} adsorption on SAM-modified Au(111) suggested displacement of thiol molecules with a direct binding of C_{60} to Au(111),[41,42] while adsorption on top of the SAM has been assumed in the earlier work.[39,40] In both cases, no direct evidence of either adsorption mode was provided. To address the question of the fate of a SAM upon C_{60} adsorption, we have characterized, using XPS, PFBT SAMs before and after adsorption of C_{60} molecules (Figure 7).

A slight decrease in the intensity of F 1s, S 2p, and Au 4f peaks was observed upon deposition of C_{60} molecules. This could originate from either overlayer adsorption (attenuating the ejected core electrons) or displacement of PFBT molecules. However, the unchanging F/Au and S/Au ratios of peak areas before and after C_{60} adsorption indicate that the PFBT SAM is intact (Figure 7d). Deconvolution of the C 1s peak reveals two main peaks, C−C at 285 eV and C−F at 287 eV, and a very small broad peak at 289 eV likely attributed to traces of C═O impurities. The C−F/Au signal remains constant, while the intensity of the C−C/Au signal increases upon C_{60} adsorption. Accordingly, we conclude that C_{60} forms an overlayer on top of the PFBT SAM.

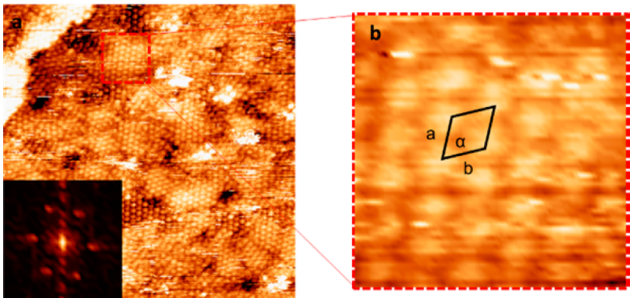

Figure 6. (a) STM image of the C_{60} layer on top of PFBT-Au (50 nm × 50 nm). The inset shows the fast Fourier transform (FFT) of the image. (b) High-resolution STM image of the highlighted area (red box). Area of 6 nm × 6 nm. Unit cell parameters are as follows: $a = b = 1.0 \pm 0.2$ nm, and $\alpha = 60 \pm 2°$. V_b = 400 mV, and I_t = 0.2 nA.

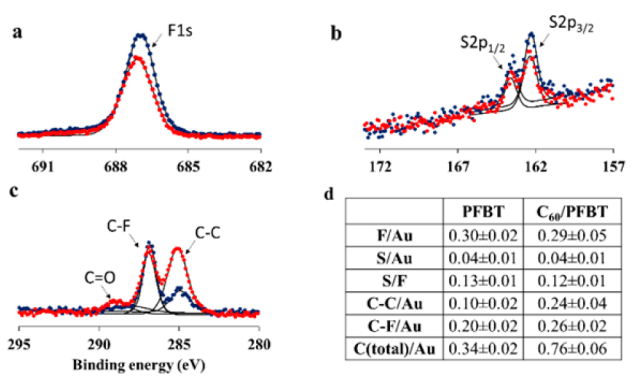

	PFBT	C_{60}/PFBT
F/Au	0.30±0.02	0.29±0.05
S/Au	0.04±0.01	0.04±0.01
S/F	0.13±0.01	0.12±0.01
C-C/Au	0.10±0.02	0.24±0.04
C-F/Au	0.20±0.02	0.26±0.02
C(total)/Au	0.34±0.02	0.76±0.06

Figure 7. XPS spectra of (a) F 1s, (b) S 2p, and (c) C 1s peaks for PFBT (blue circles) and C_{60}-PFBT (red circles) adlayers. (d) Deduced atomic ratios of elements on PFBT- and C_{60}/PFBT-modified Au surfaces.

The analysis of the surface coverage versus time (Figure 8) provides quantitative information about the growth kinetics of the C_{60} monolayer. The sigmoidal form of the curve thereby

DOI: 10.1021/acs.chemmater.6b03527
Chem. Mater. 2016, 28, 8322−8329

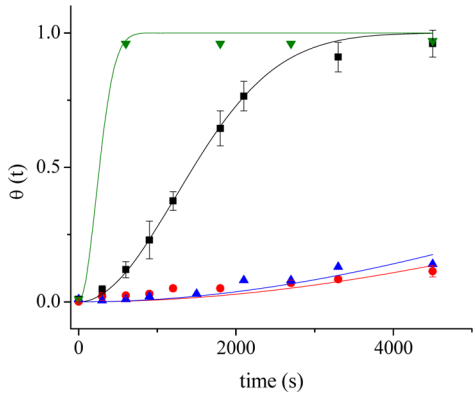

Figure 8. Evolution of molecular coverage of C_{60} adsorbed from a 1 mM solution in phenyloctane on bare Au(111) (gray triangles) and PFBT-modified (black squares), BT-modified (red circles), and C8SH-modified (black triangles) Au(111) substrates. Curves are fits to the KJMA model.

obtained is consistent with the Kolmogorov–Johnson–Mehl–Avrami (KJMA)[56,57] kinetic model (eq 1):

$$\theta(t) = 1 - e^{-kt^n} \quad (1)$$

where $\theta(t)$ is the surface coverage at time t and k is an observed rate constant that depends on both the nucleation and growth rate. The exponent n represents the dimensionality of the growth and the time dependence nucleation that was fixed at 2 (for a "free order" fitting, see Table S2). This model, originally devised to describe phase transitions in metal alloys,[58] has been recently used to predict the kinetics of self-assembled monolayer formation by molecular exchange.[59,60]

The sigmoidal shape of the adsorption isotherm cannot be fit with Langmuir adsorption models that are typically used for predicting the kinetics of SAM formation[61] (Figure S6). The better suitability of the KJMA model over Langmuir models can be attributed to the slow nucleation process of C_{60} assembly.[62] Fitting the curves to the KJMA model leads to k values of $(3.3 \pm 0.2) \times 10^{-7}$, $(9.5 \pm 1.0) \times 10^{-9}$, $(7.2 \pm 1.0) \times 10^{-9}$, and $\geq 1 \times 10^{-5}$ s^{-1} for PFBT, C8SH, BT, and Au, respectively (Table S3).

The spontaneous adsorption of C_{60} onto Au(111) has been previously attributed to the strong covalent character of C_{60}–Au interaction as demonstrated by temperature-programmed desorption (TPD)[63] (~43 kcal/mol) and DFT calculations (~31 kcal/mol).[64] However, the much faster growth of C_{60} on PFBT SAMs (as compared to BT and C8SH) was surprising in light of the hydro/lipophobic "reputation" of fluoroorganic surfaces.

Indeed, the water contact angle on BT and PFBT SAMs [75 ± 2° and 80 ± 2°, respectively (lit.[16] 74 ± 2° and 86 ± 2°, respectively)] suggests that the PFBT surface is slightly more hydrophobic than the BT surface. On the other hand, both SAMs appeared to be lipophilic on the basis of the low wetting contact angle measured for phenyloctane (<10° for both). The high lipophilicity of the PFBT SAM was somewhat unexpected considering the pronounced lipophobic properties of other fluorocarbons (hexadecane contact angle of 71° on hexafluorodecanethiol-modified Au).[65]

In the context of interactions of PFBT SAM with the environment, the large dipole moment of the PFBT molecule appears as a highly relevant feature. Although C_{60} itself is not polar, it is a legendary polarizable molecule,[66] lending itself to dipole-induced dipole interactions. The attractive electrostatic C–F···C_{60} interactions could thus be a plausible driving force for the enhanced C_{60} assembly on top of the PFBT SAM. Indeed, a crystallographic study of a series of C_{60}/C_{70} cocrystals with tetrakis(pentafluorophenyl)porphyrins revealed multiple C–F···π contacts with F···C distances as short as 2.66 Å (cf. 3.17 Å for the sum of van der Waals radii of C and F).[67]

To shed further light on the nature of the C_{60}–SAM interactions, we performed DFT calculations with empirical dispersion correction (Supporting Information). Figure 9 shows

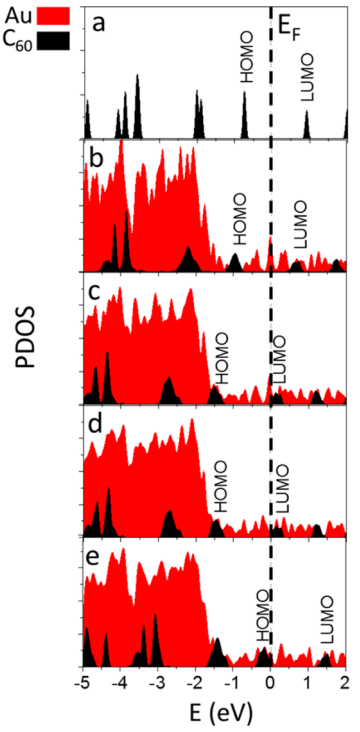

Figure 9. Projected DOS of C_{60} (a) in vacuum, (b) on Au(111), (c) on C8SH–Au(111), (d) on BT–Au(111), and (e) on PFBT–Au(111).

the density of states (DOS) of C_{60} on Au and BT-, PFBT-, and C8SH-modified Au substrates. To facilitate the fingerprinting of the peaks, the energy level of Au was maintained fixed while C_{60} peaks are shifted between different SAM–Au samples. We remark that on BT–Au and C8SH–Au surfaces, the C_{60} LUMO shifts toward the Fermi level (E_F), while on PFBT–Au surfaces, the HOMO lies next to the E_F.

This is in line with the documented decrease in the work function of Au(111) in the presence of the BT SAM and its increase in the presence of the PFBT SAM.[16,17] As a result, C_{60} acts as a typical electron acceptor acquiring partial negative charge on C8SH and BT (Mulliken populations of −0.074 and −0.159, respectively). However, on PFBT SAM, C_{60} uncharacteristically acts as a donor and is predicted to acquire a small positive charge of +0.017. Such additional positive polarization of C_{60} in the proximity of negatively polarized fluorine atoms terminating the SAM surface further enhances the electrostatic interactions mentioned above. As a net effect, DFT predicts significantly stronger binding of C_{60} to the PFBT SAM (−1.39 eV) than to BT (−0.98 eV) and C8SH (−0.59 eV) SAMs. It is noteworthy that a related effect of charge transfer on self-assembly of another electron acceptor molecule [tetracyanoquinodimethane (TCNQ)] has also been observed by STM.[68]

DOI: 10.1021/acs.chemmater.6b03527
Chem. Mater. 2016, 28, 8322–8329

CONCLUSIONS

The adsorption of C_{60} molecules onto C8SH-, BT-, and PFBT-modified Au(111) surfaces has been investigated via STM at the liquid−solid interface. Using X-ray photoelectron spectroscopy (XPS), we demonstrate that, in contrast to previous reports, the thiol adsorbates are not displaced during C_{60} adsorption but instead form a closely packed hexagonal lattice with a $(2\sqrt{3} \times 2\sqrt{3})R30°$ structure on top of the PFBT SAM. *In situ* STM characterization reveals that, in spite of the high degree of structural similarity, BT and PFBT SAMs have dramatically different abilities to direct the adsorption of C_{60} molecules from solution. The faster (>100-fold) growth kinetics of the C_{60} layer on PFBT compared to BT and C8SH SAMs can be attributed to dipole (SAM)-induced dipole (C_{60}) interactions. DFT calculations show an alignment of the C_{60} HOMO with the Fermi level of the PFBT-Au(111) surface and predict an inverse (small) charge transfer in which C_{60} functions as the donor. This work improves the fundamental understanding of interactions at the SAM−organic semiconductor interface (a common buried interface in organic electronic devices). It also suggests the possibility of switching of charge transfer/transport polarity in a given semiconductor through appropriate surface engineering.

ASSOCIATED CONTENT

Supporting Information

The Supporting Information is available free of charge on the ACS Publications website at DOI: 10.1021/acs.chemmater.6b03527.

Experimental and computational details, additional STM images, a summary of literature-reported unit cells for BT SAMs, and details of adsorption isotherm fitting (PDF)

A movie of sequential STM scans during *in-situ* adsorption of C_{60} on PFBT@Au (corresponding to Figure 4) (AVI)

AUTHOR INFORMATION

Corresponding Authors

*E-mail: bruce.lennox@mcgill.ca.

*E-mail: dmitrii.perepichka@mcgill.ca.

Notes

The authors declare no competing financial interest.

ACKNOWLEDGMENTS

This work was funded by NSERC Discovery and FQRNT Team grants (to R.B.L. and D.F.P.). M.A.M. thanks NSERC and FQRNT for doctoral fellowships. E.H.S. acknowledges funding from a NSERC Discovery grant and the Research Excellence Program of the Ontario Research Fund. We thank Pelayo Garcia de Arquer for help with experiments. Computations were performed using the BlueGene/Q supercomputer at the SciNet HPC Consortium provided through the Southern Ontario Smart Computing Innovation Platform (SOSCIP).

REFERENCES

(1) Love, J. C.; Estroff, L. A.; Kriebel, J. K.; Nuzzo, R. G.; Whitesides, G. M. Self-Assembled Monolayers of Thiolates on Metals as a Form of Nanotechnology. *Chem. Rev.* **2005**, *105*, 1103−1170.

(2) Smith, R. K.; Lewis, P. A.; Weiss, P. S. Patterning Self-Assembled Monolayers. *Prog. Surf. Sci.* **2004**, *75*, 1−68.

(3) Vericat, C.; Vela, M. E.; Benitez, G.; Carro, P.; Salvarezza, R. C. Self-Assembled Monolayers of Thiols and Dithiols on Gold: New Challenges for a Well-Known System. *Chem. Soc. Rev.* **2010**, *39*, 1805−1834.

(4) Gooding, J. J.; Mearns, F.; Yang, W.; Liu, J. Self-Assembled Monolayers into the 21st Century: Recent Advances and Applications. *Electroanalysis* **2003**, *15*, 81−96.

(5) Xia, Y.; Whitesides, G. M. Soft Lithography. *Angew. Chem., Int. Ed.* **1998**, *37*, 550−575.

(6) Lio, A.; Charych, D. H.; Salmeron, M. Comparative Atomic Force Microscopy Study of the Chain Length Dependence of Frictional Properties of Alkanethiols on Gold and Alkylsilanes on Mica. *J. Phys. Chem. B* **1997**, *101*, 3800−3805.

(7) Scherer, J.; Vogt, M. R.; Magnussen, O. M.; Behm, R. J. Corrosion of Alkanethiol-Covered Cu(100) Surfaces in Hydrochloric Acid Solution Studied by in-Situ Scanning Tunneling Microscopy. *Langmuir* **1997**, *13*, 7045−7051.

(8) Campbell, I.; Rubin, S.; Zawodzinski, T.; Kress, J.; Martin, R.; Smith, D.; Barashkov, N.; Ferraris, J. P. Controlling Schottky Energy Barriers in Organic Electronic Devices using Self-Assembled Monolayers. *Phys. Rev. B: Condens. Matter Mater. Phys.* **1996**, *54*, R14321−R14324.

(9) Meijer, E. J.; de Leeuw, D. M.; Setayesh, S.; van Veenendaal, E.; Huisman, B. H.; Blom, P. W. M.; Hummelen, J. C.; Scherf, U.; Klapwijk, T. M. Solution-Processed Ambipolar Organic Field-Effect Transistors and Inverters. *Nat. Mater.* **2003**, *2*, 678−682.

(10) De Boer, B.; Hadipour, A.; Mandoc, M. M.; van Woudenbergh, T.; Blom, P. W. M. Tuning of Metal Work Functions with Self-Assembled Monolayers. *Adv. Mater.* **2005**, *17*, 621−625.

(11) Cao, J.; Yin, J.; Yuan, S.; Zhao, Y.; Li, J.; Zheng, N. Thiols as Interfacial Modifiers to Enhance the Performance and Stability of Perovskite Solar Cells. *Nanoscale* **2015**, *7*, 9443−9447.

(12) Evans, S. D.; Ulman, A. Surface potential studies of alkyl-thiol monolayers adsorbed on gold. *Chem. Phys. Lett.* **1990**, *170*, 462−466.

(13) Alloway, D. M.; Hofmann, M.; Smith, D. L.; Gruhn, N. E.; Graham, A. L.; Colorado, R.; Wysocki, V. H.; Lee, T. R.; Lee, P. A.; Armstrong, N. R. Interface Dipoles Arising from Self-Assembled Monolayers on Gold: UV−Photoemission Studies of Alkanethiols and Partially Fluorinated Alkanethiols. *J. Phys. Chem. B* **2003**, *107*, 11690−11699.

(14) Bock, C.; Pham, D. V.; Kunze, U.; Käfer, D.; Witte, G.; Wöll, C. Improved Morphology and Charge Carrier Injection in Pentacene Field-Effect Transistors with Thiol-Treated Electrodes. *J. Appl. Phys.* **2006**, *100*, 114517.

(15) Bumm, L. A.; Arnold, J. J.; Cygan, M. T.; Dunbar, T. D.; Burgin, T. P.; Jones, L.; Allara, D. L.; Tour, J. M.; Weiss, P. S. Are Single Molecular Wires Conducting? *Science* **1996**, *271*, 1705−1707.

(16) Tatara, S.; Kuzumoto, Y.; Kitamura, M. Surface Properties of Substituted-Benzenethiol Monolayers on Gold and Silver: Work Fnction, Wettability, and Surface Tension. *Jpn. J. Appl. Phys.* **2016**, *55*, 03DD02.

(17) Nouchi, R.; Tanimoto, T. Substituent-Controlled Reversible Switching of Charge Injection Barrier Heights at Metal/Organic Semiconductor Contacts Modified with Disordered Molecular Monolayers. *ACS Nano* **2015**, *9*, 7429−7439.

(18) Smith, J.; Hamilton, R.; Qi, Y.; Kahn, A.; Bradley, D. D. C.; Heeney, M.; McCulloch, I.; Anthopoulos, T. D. The Influence of Film Morphology in High-Mobility Small-Molecule:Polymer Blend Organic Transistors. *Adv. Funct. Mater.* **2010**, *20*, 2330−2337.

(19) Li, R.; Ward, J. W.; Smilgies, D.-M.; Payne, M. M.; Anthony, J. E.; Jurchescu, O. D.; Amassian, A. Direct Structural Mapping of Organic Field-Effect Transistors Reveals Bottlenecks to Carrier Transport. *Adv. Mater.* **2012**, *24*, 5553−5558.

(20) Youn, J.; Dholakia, G. R.; Huang, H.; Hennek, J. W.; Facchetti, A.; Marks, T. J. Influence of Thiol Self-Assembled Monolayer Processing on Bottom-Contact Thin-Film Transistors Based on n-Type Organic Semiconductors. *Adv. Funct. Mater.* **2012**, *22*, 1856−1869.

(21) Kim, C. H.; Hlaing, H.; Carta, F.; Bonnassieux, Y.; Horowitz, G.; Kymissis, I. Templating and Charge Injection from Copper Electrodes into Solution-Processed Organic Field-Effect Transistors. *ACS Appl. Mater. Interfaces* **2013**, *5*, 3716−3721.

(22) Kang, C. M.; Wade, J.; Yun, S.; Lim, J.; Cho, H.; Roh, J.; Lee, H.; Nam, S.; Bradley, D. D.; Kim, J. S.; Lee, C. 1 GHz Pentacene Diode

DOI: 10.1021/acs.chemmater.6b03527
Chem. Mater. 2016, 28, 8322−8329

Rectifiers Enabled by Controlled Film Deposition on SAM-Treated Au Anodes. *Adv. Electron. Mater.* **2016**, *2*, 1500282.
(23) Ward, J. W.; Loth, M. A.; Kline, R. J.; Coll, M.; Ocal, C.; Anthony, J. E.; Jurchescu, O. D. Tailored Interface for Self-Patterning Organic Thin-Film Transistors. *J. Mater. Chem.* **2012**, *22*, 19047−19053.
(24) Park, H.; Park, J.; Lim, A.; Anderson, E.; Alivisatos, A.; McEuen, P. Nanomechanical oscillations in a single-C_{60} transistor. *Nature* **2000**, *407*, 57−60.
(25) Yu, G.; Gao, J.; Hummelen, J. C.; Wudl, F.; Heeger, A. J. Polymer Photovoltaic Cells: Enhanced Efficiencies via a Network of Internal Donor-Acceptor Heterojunctions. *Science* **1995**, *270*, 1789−1791.
(26) Mutolo, K. L.; Mayo, E. I.; Rand, B. P.; Forrest, S. R.; Thompson, M. E. Enhanced Open-Circuit Voltage in Subphthalocyanine/C_{60} Organic Photovoltaic Cells. *J. Am. Chem. Soc.* **2006**, *128*, 8108−8109.
(27) Campoy-Quiles, M.; Ferenczi, T.; Agostinelli, T.; Etchegoin, P. G.; Kim, Y.; Anthopoulos, T. D.; Stavrinou, P. N.; Bradley, D. D. C.; Nelson, J. Morphology Evolution via Self-Organization and Lateral and Vertical Diffusion in Polymer: Fullerene Solar Cell Blends. *Nat. Mater.* **2008**, *7*, 158−164.
(28) Wilson, R. J.; Meijer, G.; Bethune, D. S.; Johnson, R. D.; Chambliss, D. D.; de Vries, M. S.; Hunziker, H. E.; Wendt, H. R. Imaging C_{60} Clusters on a Surface Using a Scanning Tunnelling Microscope. *Nature* **1990**, *348*, 621−622.
(29) Altman, E. I.; Colton, R. Determination of the Orientation of C_{60} Adsorbed on Au(111) and Ag(111). *Phys. Rev. B: Condens. Matter Mater. Phys.* **1993**, *48*, 18244−18249.
(30) Sau, J. D.; Neaton, J. B.; Choi, H. J.; Louie, S. G.; Cohen, M. L. Electronic Energy Levels of Weakly Coupled Nanostructures: C_{60}-Metal Interfaces. *Phys. Rev. Lett.* **2008**, *101*, 026804.
(31) Larsson, J. A.; Elliott, S. D.; Greer, J. C.; Repp, J.; Meyer, G.; Allenspach, R. Orientation of Individual C_{60} Molecules Adsorbed on Cu(111): Low-Temperature Scanning Tunneling Microscopy and Density Functional Calculations. *Phys. Rev. B: Condens. Matter Mater. Phys.* **2008**, *77*, 115434.
(32) Bonifazi, D.; Salomon, A.; Enger, O.; Diederich, F.; Cahen, D. Tuning Electronic Properties of Semiconductors by Adsorption of [60]Fullerene Carboxylic Acid Derivatives. *Adv. Mater.* **2002**, *14*, 802−805.
(33) Sánchez-Sánchez, C.; Lanzilotto, V.; González, C.; Verdini, A.; de Andrés, P. L.; Floreano, L.; López, M. F.; Martín-Gago, J. A. Weakly Interacting Molecular Layer of Spinning C60 Molecules on TiO_2 (110) Surfaces. *Chem. - Eur. J.* **2012**, *18*, 7382−7387.
(34) Yao, X.; Ruskell, T. G.; Workman, R. K.; Sarid, D.; Chen, D. Scanning Tunneling Microscopy and Spectroscopy of Individual C_{60} Molecules on Si(100)-(2 × 1) Surfaces. *Surf. Sci.* **1996**, *366*, L743−L749.
(35) Bonifazi, D.; Spillmann, H.; Kiebele, A.; de Wild, M.; Seiler, P.; Cheng, F.; Güntherodt, H.-J.; Jung, T.; Diederich, F. Supramolecular Patterned Surfaces Driven by Cooperative Assembly of C_{60} and Porphyrins on Metal Substrates. *Angew. Chem., Int. Ed.* **2004**, *43*, 4759−4763.
(36) Mena-Osteritz, E.; Bäuerle, P. Complexation of C_{60} on a Cyclothiophene Monolayer Template. *Adv. Mater.* **2006**, *18*, 447−451.
(37) MacLeod, J. M.; Ivasenko, O.; Fu, C.; Taerum, T.; Rosei, F.; Perepichka, D. F. Supramolecular Ordering in Oligothiophene−Fullerene Monolayers. *J. Am. Chem. Soc.* **2009**, *131*, 16844−16850.
(38) Yang, Y.-C.; Chang, C.-H.; Lee, Y.-L. Complexation of Fullerenes on a Pentacene-Modified Au(111) Surface. *Chem. Mater.* **2007**, *19*, 6126−6130.
(39) Zeng, C. G.; Wang, H. Q.; Wang, B.; Yang, J. L.; Hou, J. G. Negative Differential-Resistance Device Involving Two C_{60} Molecules. *Appl. Phys. Lett.* **2000**, *77*, 3595−3597.
(40) Zeng, C. G.; Wang, B.; Li, B.; Wang, H. Q.; Hou, J. G. Self-Assembly of One-Dimensional Molecular and Atomic Chains Using Striped Alkanethiol Structures as Templates. *Appl. Phys. Lett.* **2001**, *79*, 1685−1687.
(41) Li, F.; Tang, L.; Zhou, W.; Guo, Q. Formation of Confined C_{60} Islands within Octanethiol Self-Assembled Monolayers on Au(111). *J. Phys. Chem. C* **2009**, *113*, 17899−17903.
(42) Nakayama, M.; Kautz, N. A.; Wang, T.; Sibener, S. J. Formation of Rectangular Packing and One-Dimensional Lines of C_{60} on 11-Phenoxyundecanethiol Self-Assembled Monolayers on Au(111). *Langmuir* **2012**, *28*, 4694−4701.
(43) Hong, S.-Y.; Yeh, P.-C.; Dadap, J. I.; Osgood, R. M. Interfacial Dipole Formation and Surface-Electron Confinement in Low-Coverage Self-Assembled Thiol Layers: Thiophenol and p-Fluorothiophenol on Cu(111). *ACS Nano* **2012**, *6*, 10622−10631.
(44) Tao, Y.-T.; Wu, C.-C.; Eu, J.-Y.; Lin, W.-L.; Wu, K.-C.; Chen, C.-H. Structure Evolution of Aromatic-Derivatized Thiol Monolayers on Evaporated Gold. *Langmuir* **1997**, *13*, 4018−4023.
(45) Yang, G. H.; Liu, G. Y. New Insights for Self-Assembled Monolayers of Organothiols on Au(111) Revealed by Scanning Tunneling Microscopy. *J. Phys. Chem. B* **2003**, *107*, 8746−8759.
(46) Wan, L.-J.; Terashima, M.; Noda, H.; Osawa, M. Molecular Orientation and Ordered Structure of Benzenethiol Adsorbed on Gold(111). *J. Phys. Chem. B* **2000**, *104*, 3563−3569.
(47) Kang, H.; Park, T.; Choi, I.; Lee, Y.; Ito, E.; Hara, M.; Noh, J. Formation of Large Ordered Domains in Benzenethiol Self-Assembled Monolayers on Au(111) Observed by Scanning Tunneling Microscopy. *Ultramicroscopy* **2009**, *109*, 1011−1014.
(48) Kang, H.; Lee, H.; Kang, Y.; Hara, M.; Noh, J. Two-Dimensional Ordering of Benzenthiol Self-Assembled Monolayers Guided by Displacement of Cyclohexanethiols on Au(111). *Chem. Commun.* **2008**, 5197−5199.
(49) Azzam, W.; Bashir, A.; Ulrich Biedermann, P.; Rohwerder, M. Formation of Highly Ordered and Orientated Gold Islands: Effect of Immersion Time on the Molecular Adlayer Structure of Pentafluorobenzenethiols (PFBT) SAMs on Au(111). *Langmuir* **2012**, *28*, 10192−10208.
(50) Kang, H.; Lee, N.-S.; Ito, E.; Hara, M.; Noh, J. Formation and Superlattice of Long-Range-Ordered Self-Assembled Monolayers of Pentafluorobenzenethiols on Au(111). *Langmuir* **2010**, *26*, 2983−2985.
(51) Maksymovych, P.; Voznyy, O.; Dougherty, D. B.; Sorescu, D. C.; Yates, J. T., Jr. Gold Adatoms as a Key Structural Component in Self-Assembled Monolayers of Organosulfur Molecules on Au(111). *Prog. Surf. Sci.* **2010**, *85*, 206−240.
(52) Pawlak, R.; Kawai, S.; Fremy, S.; Glatzel, T.; Meyer, E. High-Resolution Imaging of C_{60} Molecules Using Tuning-Fork-Based Non-contact Atomic Force Microscopy. *J. Phys.: Condens. Matter* **2012**, *24*, 084005.
(53) Bommel, S.; Kleppmann, N.; Weber, C.; Spranger, H.; Schäfer, P.; Novak, J.; Roth, S. V.; Schreiber, F.; Klapp, S. H. L.; Kowarik, S. Unravelling the Multilayer Growth of the Fullerene C_{60} in Real Time. *Nat. Commun.* **2014**, *5*, 5388−5395.
(54) Zhong, D.; Hirtz, M.; Wang, W.; Dou, R.; Chi, L.; Fuchs, H. Kinetics of Island Formation in Organic Film Growth. *Phys. Rev. B: Condens. Matter Mater. Phys.* **2008**, *77*, 113404.
(55) Xiao, W. D.; Ruffieux, P.; Ait-Mansour, K.; Groning, O.; Palotas, K.; Hofer, W. A.; Groning, P.; Fasel, R. Formation of a Regular Fullerene Nanochain Lattice. *J. Phys. Chem. B* **2006**, *110*, 21394−21398.
(56) Khawam, A.; Flanagan, D. R. Solid-State Kinetic Models: Basics and Mathematical Fundamentals. *J. Phys. Chem. B* **2006**, *110*, 17315−17328.
(57) Finney, E. E.; Finke, R. G. Is There a Minimal Chemical Mechanism Underlying Classical Avrami-Erofe'ev Treatments of Phase-Transformation Kinetic Data? *Chem. Mater.* **2009**, *21*, 4692−4705.
(58) Avrami, M. Kinetics of Phase Change. II. Transformation-Time Relations for Random Distribution of Nuclei. *J. Chem. Phys.* **1940**, *8*, 212−224.
(59) Saavedra, H. M.; Barbu, C. M.; Dameron, A. A.; Mullen, T. J.; Crespi, V. H.; Weiss, P. S. 1-Adamantanethiolate Monolayer Displacement Kinetics Follow a Universal Form. *J. Am. Chem. Soc.* **2007**, *129*, 10741−10746.
(60) Hohman, J. N.; Thomas, J. C.; Zhao, Y.; Auluck, H.; Kim, M.; Vijselaar, W.; Kommeren, S.; Terfort, A.; Weiss, P. S. Exchange Reactions between Alkanethiolates and Alkaneselenols on Au{111}. *J. Am. Chem. Soc.* **2014**, *136*, 8110−8121.

DOI: 10.1021/acs.chemmater.6b03527
Chem. Mater. 2016, 28, 8322−8329

(61) Kassam, A.; Bremner, G.; Clark, B.; Ulibarri, G.; Lennox, R. B. Place Exchange Reactions of Alkyl Thiols on Gold Nanoparticles. *J. Am. Chem. Soc.* **2006**, *128*, 3476−3477.
(62) Dill, E. D.; Folmer, J. C.; Martin, J. D. Crystal Growth Simulations to Establish Physically Relevant Kinetic Parameters from the Empirical Kolmogorov−Johnson−Mehl−Avrami Model. *Chem. Mater.* **2013**, *25*, 3941−3951.
(63) Tzeng, C. T.; Lo, W. S.; Yuh, J. Y.; Chu, R. Y.; Tsuei, K. D. Photoemission, Near-Edge x-ray-Absorption Spectroscopy, and Low-Energy Electron-Diffraction Study of C_{60} on Au(111) Surfaces. *Phys. Rev. B: Condens. Matter Mater. Phys.* **2000**, *61*, 2263−2272.
(64) Li, H.; Pussi, K.; Hanna, K.; Wang, L.-L.; Johnson, D.; Cheng, H. P.; Shin, H.; Curtarolo, S.; Moritz, W.; Smerdon, J.; McGrath, R.; Diehl, R. Surface Geometry of C_{60} on Ag(111). *Phys. Rev. Lett.* **2009**, *103*, 056101.
(65) Bain, C. D.; Troughton, E. B.; Tao, Y. T.; Evall, J.; Whitesides, G. M.; Nuzzo, R. G. Formation of Monolayer Films by the Spontaneous Assembly of Organic Thiols from Solution onto Gold. *J. Am. Chem. Soc.* **1989**, *111*, 321−335.
(66) Sabirov, D. S. Polarizability as a Landmark Property for Fullerene Chemistry and Materials Science. *RSC Adv.* **2014**, *4*, 44996−45028.
(67) Olmstead, M. M.; Nurco, D. J. Fluorinated Tetraphenylporphyrins as Cocrystallizing Agents for C_{60} and C_{70}. *Cryst. Growth Des.* **2006**, *6*, 109−113.
(68) Tseng, T.-C.; Urban, C.; Wang, Y.; Otero, R.; Tait, S. L.; Alcami, M.; Ecija, D.; Trelka, M.; Gallego, J. M.; Lin, N.; Konuma, M.; Starke, U.; Nefedov, A.; Langner, A.; Woll, C.; Herranz, M. A.; Martin, F.; Martin, N.; Kern, K.; Miranda, R. Charge-Transfer-Induced Structural Rearrangements at Both Sides of Organic/Metal Interfaces. *Nat. Chem.* **2010**, *2*, 374−379.

■ NOTE ADDED AFTER ASAP PUBLICATION

This paper was published ASAP on October 25, 2016, with an incorrect Supporting Information file. The corrected version was published ASAP on October 27, 2016.

DOI: 10.1021/acs.chemmater.6b03527
Chem. Mater. 2016, 28, 8322−8329